Effect of graphene addition on the mechanical and electrical properties of Al2O3-SiCw ceramics

S. Grigoriev[a], P. Peretyagin[a], A. Smirnov[a], W. Solís [a], L.A. Díaz[b], A. Fernández[b], R. Torrecillas [a,b]

a Moscow State University of Technology "STANKIN", Vadkovskij per. 1, Moscow, 101472, Russian Federation

b Nanomaterials and Nanotechnology Research Centre (CINN), CSIC-Universidad de Oviedo, 33940 El Entrego, Principado de Asturias, Spain

Abstract

This paper presents a study on graphene-reinforced Al2O3-SiCw ceramic composites and the relationship between graphene oxide (GO) loading and the resulting mechanical and electrical properties. Well-dispersed ceramic-GO powders were fabricated using a colloidal processing route. Dense composites were obtained via spark plasma sintering, a technique that has the ability to reduce GO to graphene in situ during the sintering process. The mechanical properties of the sintered composites were investigated. The composite with only a small amount of graphene (0.5 vol.%) showed the highest flexural strength (904 ± 56 MPa), fracture toughness (10.6 ± 0.3 MPa·m1/2) and hardness (22 ± 0.8 GPa) with an extremely good dispersion of graphene within the ceramic matrix. In addition to these exceptional mechanical properties, the sintered composites also showed high electrical conductivity, which allows the compacts to be machined using electrical discharge machining and thus facilitates the fabrication of ceramic components with sophisticated shapes while reducing machining costs.

1. Introduction

Al2O3-SiC composites are very promising as structural components [1–3] and as wear-resistant elements, e.g., cutting tools and forming dies [4–7]. The inclusion of a secondary phase (SiC) into an alumina ceramic matrix can result in higher fracture toughness and strength when compared to the monolithic ceramic [2,8,9], the level of toughening being strongly dependent on the morphology of the second phase (i.e., particles, whiskers, or fibres [10,11]). Unfortunately, silicon carbide/alumina composites are difficult to densify due to the covalent nature of the SiC bond. In the case of pressure-less sintering, high sintering temperatures are usually required for the fabrication of fully dense Al2O3-SiC nanocomposites. However, the use of high sintering temperatures accelerates grain boundary diffusion, resulting in coarser grained microstructures. Therefore, Spark Plasma Sintering (SPS) was used in order to reduce sintering temperature and avoid undesirable grain growth. SPS is a fast solidification technique that allows high quality and uniform compacts to be sintered rapidly at lower temperatures than those used in more conventional sintering methods. The main advantages of the SPS process include: (i) nanostructure preservation, (ii) significant reduction of consolidation times and a short powder densification time due to the synergetic combination of electrical energy and mechanical pressure, and (iii) preservation of starting powder properties, allowing the cost-effective fabrication of bulk nanocomposites [12]. Additionally, the commercial application of these nanocomposites requires the use of mastered and reliable manufacturing technologies. Traditional machining processes use hard tools or abrasive materials to remove softer materials and create the desired final shape. However, the intrinsic high hard-ness and brittleness of ceramics coupled with their lack of electrical conductivity makes conventional machining of ceramics very difficult or even impossible. Thus, alternative machining processes are required. Electrical discharge

machining (EDM) is a technique that can be applied to successfully machine single-phase ceramics, cermets and ceramic matrix composites [13]. An important feature of EDM machining is that it can only be employed with electrically conductive materials. Electrical discharge machining requires the material to have an electrical resistivity below 100–300 Ω cm for efficient machining [14]. Unfortunately, aluminium oxide and silicon carbide have higher resistivity and, consequently, cannot be machined by EDM. In order to increase the electrical conductivity of these ceramics, graphene oxide (GO) was added to the corresponding ceramic matrices. GO processing shows several key advantages when compared with graphene, such as: i) it can be obtained in high quantities through a low-cost method ii) as an oxide it can be homogeneously dispersed in water, and, consequently, iii) mixtures of graphene oxide with any ceramic oxide can be processed following conventional ceramic processing routes. In addition to this, a small volume fraction of graphene makes it possible to reach the percolation threshold of the sample, turning it into a conductive material. The purpose of the present study was to obtain dense electro conductive whisker-reinforced Al2O3-SiC ceramic composites with different GO concentrations and describe the influence of GO on the mechanical and electrical properties of these newly developed composites.

2. Materials and characterization

2.1. Raw materials

Ceramtuff (grade HA9S) “ready-to-press powder”, a commercial blend of alumina (Al2O3) powder and 17 vol.% of silicon carbide whiskers (SiCw), fabricated by the company Advanced Composite Materials, LLC (Greer, SC, USA), was chosen for the production of ceramic-graphene composites. The typical properties of HA9S after sintering by hot press at 1850◦C are presented in Table 1.

2.2. Powder processing and sintering

Graphene oxide was synthesized by using a modified Hummers method through oxidation of graphite powder [15,16]. Briefly, this method employs Hummers reagents with small amounts of NaNO3 and KMnO4. Concentrated H2SO4 was added to a mixture of synthetic graphite and NaNO3, and the mixture was cooled down using an ice bath. Afterwards, KMnO4 was slowly added, in small doses, to keep the reaction temperature below 20ºC. The solution was then heated to 35ºC and stirred for 3 h. At that point, a hydrogen peroxide (H2O2) solution 3% was slowly poured onto the mixture, giving rise to a pronounced exothermal effect up to 98◦C. The reaction mixture was stirred for 30 min and centrifuged (3700 rpm for30 min) to discard the supernatant. The remaining solid material was then washed with water and centrifuged again; this process was repeated until reaching neutral pH. A colloidal suspension of individual graphene oxide sheets in purified water (1 mg mL−1)was prepared in 1 L batches and sonicated for 10 h. Afterwards, the suspension was centrifuged (3700 rpm for 30 min) to discard the filtered supernatant. Starting from the commercially available Ceramtuff blend, four powder mixtures containing different amounts of GO were pre-pared using a colloidal method. Al2O3-SiCw powders were added to 100 mL of water at a pH 10, previously fixed by adding NH4OH.The Al2O3-SiCw powder was dispersed by stirring for 30 min. Then, the appropriate amount of the graphene oxide suspension was dropwise to the ceramic powder dispersions. The mixed powder suspensions were stirred for 1 h. In order to prevent GO agglomeration during drying, the suspensions were dried in a FreeZone2.5 freeze-drying system (LabConco, Kansas, MO, USA). The col-lector temperature is continuously set at −50 ± 2◦C. Furthermore, the shell temperature and the chamber pressure were kept at+23 ± 2ºC and 0.02 ± 0.01 mbar, respectively, during the entire pro-cess. This method makes it is possible to obtain a homogeneous and agglomerate-free

dispersion of GO and SiC particles inside the alumina matrix without sieving. Powder densification was performed by SPS (FCT Systeme GmbH, KCE FCT-H HP D-25 SD, Rauenstein, Germany) at a maximum temperature of 1780ºC, reached under vacuum at a heating rate of 100ºC/min, and an applied pressure of 80 MPa. The final temperature and pressure were maintained for 3 min. Sintering temperature were chosen based on a previous study [7]. The sintered specimens had diameters of 20 and 50 mm and thicknesses of 4 mm. For comparison purposes Al2O3-SiCw powders without GO were SPSed following the same sintering cycle. Samples were labelled depending on their GO content: 0, 0.2,0.5, 1 and 5 vol.%, as: 0-G, 0.2-G, 0.5-G, 1-G and 5-G, respectively.

2.3. Microstructural characterization

Scanning electron microscopy (SEM) characterization was carried out on polished down to 1 μm and thermally etched surfaces (1250◦C for 3 min) by VEGA 3 LMH (SEM Tescan, Brno, CzechRepublic). The density of the sintered samples (ρ) was measured in distilled water using Archimedes' principle and was compared with the theoretical value, calculated according to the rule of mixtures. Raman spectra of as-prepared powders and sintered samples were collected to identify the phase composition. The Raman setup is composed of a laser (DXRTM2 Raman Microscope, Thermo Fisher Scientific, MA, USA) with a wavelength of 532 nm and a laser power of 2.0 mW. The laser beam was focused through an optical micro-scope's 50× objective lens to a spot size of 50 μm on the studiedarea (from different spots, at an interval of 200 nm). The accumulation time for each Raman spectrum was about 10 s.

Vickers hardness, Hv, was measured on polished surfaces using a Vickers diamond indenter (QNess A10 Microhardness Tester, Salzburg, Austria), applying a load of 98 N and an indentation time of 10 s.

The sizes of the corresponding indentations were determined via SEM. The hardness results were averaged over 10 indentations per specimen.

Biaxial flexural strength (σf) was measured using the piston-on-3-ball method (ISO 6872 standard). Specimens (diameter: 20 mm, and thickness: 1.3–1.9 mm) with polished tensile sides were placed on three balls located 120º apart on a 10 mm diameter circle. A piston positioned above the center of the three ball support applies the load directly to the unpolished side producing a biaxial flexural loading condition. The tests were performed at room temperature with a 5 kN universal testing machine (AutoGraph AG-X, ShimadzuCorp., Kyoto, Japan) at a piston speed of 1 mm/min until failure. Twelve specimens were tested for average strength and elastic modulus calculation. Data collection details and calculation procedures have been reported elsewhere [17].

Fracture toughness (K1c) was measured using single edge notched beams (SENB, dimension 3.0 × 4.0 × 45 mm3). Tests were performed at room temperature, using the same testing machine applied for flexural strength determination, at a crosshead speed of 0.5 mm/min with a span of 40 mm. Specimens were notched with a diamond blade saw. The method and formulas for calculating K1c have been reported elsewhere [18].

2.4. Measurement of electrical resistance

The d.c. resistivity variation of the samples (3 × 4 × 18 mm3) as a function of GO content was measured using a two-channel nano-voltmeter (Keithley 2182A, Cleveland, OH, USA) with silver paste contacts and a separate current source (Keithley 6220, Cleveland, OH, USA).

3. Results and discussion

3.1. Microstructure and Raman characterization

Raman spectroscopy has proven to be a useful tool to evaluate the thermal reduction of graphene oxide throughout the composite. Fig. 1 shows the Raman spectra of the raw powder mixtures and the sintered compositions.

Fig. 1a–d shows the Raman spectra that correspond to the mixtures before sintering by SPS; they reveal that all compositions consist of alumina, silicon carbide and typical GO peaks. The broad G peak and negligible second order region are characteristic of sp1, sp2 and sp3 hybridized carbon–carbon bonds in graphene [19]. The D bands at ∼1350 cm−1 confirm the lattice distortions [20]. The intensity of the GO peaks increases with increasing GO content. For the material that was sintered at 1780ºC (Fig. 1e–h), the intensity of the D band, associated with disorder, decreases while the intensity of the G band, observed in graphitic structures, increases. In addition, a well-resolved 2D symmetric peak appears at ∼2700 cm−1. These results indicate that the thermal reduction (including the restoration of large sp2regions) of graphene oxide is favoured by SPS at 1780◦C.

Fig. 2 shows representative microstructures of the sintered samples. As can be observed, SiCw are homogeneously distributed inside the alumina matrix. The darkest areas correspond to alumina and the intermediate grey phase corresponds to SiCw. It has to be noted that, due to the soft ball mixing process, the samples containing GO present a dispersion of SiC whiskers with a lower aspect ratio than the starting A2O3-SiCw powders. Only the longer whiskers are affected by this difference in the processing conditions. Small black dots are caused by ineffective polishing.

Concerning alumina grain size, the addition of a GO second phase clearly affects matrix grain growth during sintering. Fig. 3 shows a set of microstructures corresponding to thermally etched SPSed composites. In comparison to the pure Al2O3-SiCw sample, in

which large and uneven grains of alumina are observed, ceramic composites reinforced with GO exhibit more uniform and finer microstructures. The average grain size of alumina was deter-mined using the linear intercept method [21] and was found to be 2.4 ± 0.38 μm, 1.6 ± 0.33 μm, 1.4 ± 0.28 μm, 1.2 ± 0.24 μm and 0.7 ± 0.05 μm for the 0-G, 0.2-G, 0.5-G, 1-G and 5-G composites, respectively. Therefore, the average grain sizes of the ceramic matrix decrease with increasing GO content. This reduction in grain size can be attributed to the GO distribution between the ceramic grain boundaries preventing migration of grain boundaries, resulting in a microstructure refinement of microstructure. However, the most important microstructural feature is the change in the Al2O3-SiCw interfacial energy. Composites without graphene show how alumina grains grew during sintering surrounding SiCw crystals, taking up in many cases an intragranular position. In the case of composites with graphene it can be observed how small amounts of GO drastically modify the SiCw-Al2O3 interfacial energy reducing the number of silicon carbide whiskers in intragranular positions. In fact only in the case of 0.2-G and 0.5-G composites some whiskers in intragranular positions were maintained and for higher GO amounts only intergranular positions can be observed with a clear reduction of alumina grain size.

3.2. Mechanical properties

Fig. 4 shows the effect of GO content on the Vickers hardness(HV), fracture toughness (KIc) and flexural strength (σf) of alumina-SiCw-GO composites. This data shows that the mechanical behaviour of these composites improves with the addition of GO, reaching a maximum strength of 904 ± 56 MPa and a maximum fracture toughness of 10.6 ± 0.3 MPa·m1/2at 0.5 vol.% GO, that is, for the 0.5-G composition.

It has been published elsewhere that small amounts of graphene can improve the mechanical properties of alumina [22]. In fact, it is well known that a small amount of

graphene at alumina grain boundaries provides clear alumina R-curve behavior on alumina thanks to the weakness of grain boundaries facilitating extrinsic reinforcement mechanisms in the wake region. These mechanisms become more active with an increase of alumina grain size; how-ever, the use of graphene also has a clear inhibition effect on grain growth during sintering. This is why graphene is beneficial in very small amounts, because it introduces new reinforcement mechanisms without largely reducing alumina grain size. In the case of alumina-SiCw, the whiskers already act as an alumina grainsize inhibitor. Nevertheless, graphene can play an important role at alumina-SiCw interfaces, as a weakness of these interfaces can improve the pull out processes in these composites with small GO additions. In fact, Figs. 5 and 6 clearly show many cracks propagating through alumina and whiskers interfaces; the fracture surfaces show a more intricate surface due to a more intergranular fracture and, as a consequence, a higher fracture energy.

The Vickers hardness of composites containing GO is slightly affected by the presence of GO. The good dispersion of the graphene phase and the reduction of alumina grain size can behave as two balanced effects maintaining hardness levels despite GO addition. Only in the case of high amounts of GO (5-G composite) a clear reduction in hardness can be detected.

SEM images corresponding to the fracture surface of sintered0.5-G composites are shown in Fig. 5. This figure confirms that graphene is well dispersed in the ceramic matrix. Interfaces play a very important role in Al2O3-SiCw composites and the presence of graphene can enhance the already outstanding reinforcement that whiskers provide due to pull out processes or extrinsic reinforcement mechanisms that take place in the wake region.

Fig. 6 shows the Vickers indentation cracks induced on the surfaces of Al2O3-SiCw sample and a 0.5-G composite. Fig. 6A, corresponding to the Al2O3-SiCw sample, shows a crack path that is mainly comprised of transgranular fractures which, consequently, implies a lower fracture toughness than that of the 0.5-G composite. Graphene-reinforced ceramic matrix composites show three different types of crack paths: singly deflected crack, doubly deflected crack and penetrating crack, similar to fiber-reinforced composites (Fig. 6B). Figs. 5 and 6 show different toughening mechanisms, such as crack deflection, pullout and bridging of silicon carbide whiskers and graphene in the case of 0.5-G composites. The relatively large size of the graphene flakes located at the interfaces improves the crack deflection length. Therefore, graphene seems to be an optimum reinforcement for Al2O3-SiCw composites, as it improves the operating reinforcement mechanisms, maintains the stiffness of the material and, as a consequence, improves both toughness and fracture resistance. The best results were obtained for low graphene additions, which minimize graphene aggregation. Higher GO con-tents, of up to 5 vol.%, led to weaker mechanical properties due to graphene aggregation in the ceramic matrix and the presence of microstructural porosity (Fig. 3E).

3.3. Electrical conductivity

The electrical resistivity of the composites decreased with increasing graphene content, as shown in Fig. 7, reaching a value of2.2·Ω cm for the 5-G composition. The percolation threshold of the composites containing GO was found to be around 0.5 vol.%, indicated by the exponential increase of the electrical resistivity (up to 8 times higher in comparison to the alumina-SiCw ceramic). EDM is used for efficient machining when the materials have a a material has an electrical resistivity below 100–300 Ω·cm. Therefore,0.5-G, 1-G and 5-G compositions are suitable for EDM. In addition, electrical conductivity still increased when the graphene content was above the percolation threshold. This can be

explained by the fact that, when graphene content increases, there is an increase in the intersheet connections that cause this conductivity improvement along the a–b graphene planes (orientation: perpendicular to the pressure direction applied in SPS). In the case of materials made with CNTs, the CNTs are prone to agglomerate exceeding the percolation limit of the composite. In these agglomerates, CNTs show “point-to-point” contact geometry. As a result, the electrical resistivity increases with the degree of non-homogeneity of CNTs through the matrix. When graphene is used as the second phase in composites, the type of contact between the 2D plate-shaped particles is “area-to-area”. As a consequence, close-fitted and interconnected highly conductive graphene networks result in an improvement of electrical conductivity.

4. Conclusion

Al2O3-SiCw-graphene oxide composites (containing 0.2, 0.5,1 and 5 vol.% GO) have been successfully fabricated by combining a colloidal processing route and Spark Plasma Sintering. Results showed that the addition of low graphene oxide contents to an Al2O3-SiCw ceramic matrix simultaneously improved fracture toughness and strength. This mechanical upgrade takes place when small quantities of graphene are homogeneously dispersed in the matrix. Several extrinsic reinforcement mechanisms (crack deflection, pull-out and bridging) are promoted due to the presence of graphene at Al2O3-SiCw boundaries. The composite containing 0.5vol.% GO has the highest flexural strength (904 ± 56 MPa), fracture toughness (10.6 ± 0.3 MPa m1/2) and hardness (22 ± 0.8 GPa). Compared to Al2O3/SiCw composites without graphene oxide addition, for 0.5-G composite, the percentage increase of Vickers hardness, strength and fracture toughness reported as 4%, 29% and 10%respectively. The lower mechanical properties of the composites containing 5 vol.% GO is related to the aggregation of graphene oxide in the ceramic matrix and the presence of porosity in the final compact. In addition to these

exceptional mechanical properties, SPS-sintered Al2O3-SiCw-0.5 vol.% GO composites also showed an electrical resistivity below 100 Ω·cm, demonstrating their suitability for electrical discharge machining. Further studies are needed for investigation and theoretical modelling of the varying types of graphene/ceramic interfaces developed experimentally and their impact on the reinforcing mechanism in composite. This understanding will enable the processing and designing of most advantageous properties of these interfaces. In addition, the uniform dispersion of graphene and composite's structure retention and control which affect the microstructural evolution during processing might also represent the prospective goal for further research.

Acknowledgments

Authors would like to thank The Ministry of the Russian Federation supported this work in the frame of Governmental Regulation of the Russian Federation No. 220, 9 April 2010 by contract 14.B25.31.0012, 26 June 2013.

References

[1] Y. Quanzu, T. Troczynski, Alumina sol-assisted sintering of SiC–Al2O3composites, J. Am. Ceram. Soc. 83 (2000) 958–960.

[2] Y.L. Dong, F.M. Xu, X.L. Shi, C. Zhang, Z.J. Zhang, J.M. Yang, Y. Tana, Fabrication and mechanical properties of nano-/micro-sized Al2O3/SiC composites, Mater.Sci. Eng. A Struct. 504 (2009) 49–54.

[3] M. Parchoviansk´y, D. Galusek, J. Sedlá˘cek, P.˘Svan˘cárek, M. Ka˘siarová, J. Dusza,P.˘Sajgalík, Microstructure and mechanical properties of hot pressed Al2O3/SiC nanocomposites, J. Eur. Ceram. Soc. 33 (2013) 2291–2298.

[4] A. Smirnov, J.F. Bartolomé, J.S. Moya, F. Kern, R. Gadow, Dry reciprocating sliding wear behaviour of alumina–silicon carbide nanocomposite fabricated by ceramic injection molding, J. Eur. Ceram. Soc. 31 (2011) 469–474.

[5] J. Sedlá˘cek, D. Galusek, P.˘Svan˘cárek, R. Riedel, A. Atkinson, X. Wang, Abrasivewear of Al2O3–SiC and Al2O3–(SiC)–C composites with micrometer- and submicrometer-sized alumina matrix grains, J. Eur. Ceram. Soc. 28 (2008)2983–2993.

[6] M. Belmonte, M.I. Nieto, M.I. Osendi, P. Miranzo, Influence of the SiC grain size on the wear behaviour of Al2O3/SiC composites, J. Eur. Ceram. Soc. 26 (2006)1273–1279.

[7] C.F. Gutiérrez-González, M. Suarez, S. Pozhidaev, S. Rivera, P. Peretyagin, W.Solís, L.A. Díaz, A. Fernandez, R. Torrecillas, Effect of TiC addition on the mechanical behaviour of Al2O3–SiC whiskers composites obtained by SPS, J.Eur. Ceram. Soc. 36 (2016) 2149–2152.

[8] S.K. Sharma, B. Venkata Manoj Kumar, K.Y. Lim, Y.W. Kim, S.K. Nath, Erosion behavior of SiC–WC composites, Ceram. Int. 40 (2014) 6829–6839.

[9] K. Takahashi, M. Yokouchi, S.K. Lee, K. Ando, Crack-healing behavior of Al2O3toughened by SiC whiskers, J. Am. Ceram. Soc. 86 (2003) 2143–2147.

[10] S. Kovalev, T. Ohji, Y. Yamauchi, M. Sakai, Grain boundary strength innon-cubic ceramic polycrystals with misfitting intragranular inclusions(nanocomposites), J. Mater. Sci. (2000) 1405–1412.

[11] M. Sternitzke, B. Derby, R.J. Brook, Alumina/silicon cabride nancomposites by hybrid polymer/powder processing: microstructures and mechanical properties, J. Am. Ceram. Soc. (1998) 41–48.

[12] V. Viswanathan, T. Laha, K. Balani, A. Agarwal, S. Seal, Challenges and advances in nanocomposite processing techniques, Mater. Sci. Eng. Rep. 54(2006) 121–185.

[13] W. König, D.F. Dauw, G. Levy, U. Panten, EDM-future steps towards the machining of ceramics, CIRP Ann. Manuf. Technol. 37 (1988) 623–631.

[14] T. Rodriguez-Suarez, J.F. Bartolomé, A. Smirnov, S. Lopez-Esteban, L.A. Díaz, R.Torrecillas, J.S. Moya, Electroconductive alumina-TiC-Ni nanocomposites obtained by spark plasma sintering, Ceram. Int. (2011) 1631–1636.

[15] W.S. Hummers Jr., R.E. Offeman, Preparation of graphitic oxide, J. Am. Chem.Soc. (1958) 1339.

[16] C. Botas, A.M. Pérez-Mas, P. Álvarez, R. Santamaría, M. Granda, C. Blanco, R.Menéndez, Optimization of the size and yield of graphene oxide sheets in the exfoliation step, Carbon (2013) 576–578.

[17] A. Smirnov, J.F. Bartolomé, Microstructure and mechanical properties of ZrO2ceramics toughened by 5–20 vol.% Ta metallic particles fabricated by pressureless sintering, Ceram. Int. (2014) 1829–1834.

[18] A. Smirnov, J.F. Bartolomé, Mechanical properties and fatigue life of ZrO2-Tacomposites prepared by hot pressing, J. Eur. Ceram. Soc. (2012) 3899–3904.

[19] H.-L. Guo, X.-F. Wang, Q.-Y. Qian, F.-B. Wang, X.-H. Xia, A green approach to the synthesis of graphene nanosheets, ACS Nano 3 (2009) 2653–2659.

[20] A.C. Ferrari, J.C. Meyer, V. Scardaci, C. Casiraghi, M. Lazzeri, F. Mauri, S.Piscanec, D. Jiang, K.S. Novoselov, S. Roth, A.K. Geim, Raman spectrum ofgraphene and graphene layers, Phys. Rev. Lett. 97 (2006) 187401.

[21] J.C. Wurst, J.A. Nelson, Lineal intercept technique for measuring grain size in two-phase polycrystalline ceramics, J. Am. Ceram. Soc. 55 (1972) 109–111.

[22] A. Centeno, V.G. Rocha, B. Alonso, A. Fernández, C.F. Gutierrez-Gonzalez, R.Torrecillas, A. Zurutuza, Graphene for tough and electroconductive alumina ceramics, J. Eur. Ceram. Soc. 33 (2013) 3201–3210

Table 1 Properties of the Ceramtuff blend after densification

Density (% φ_{th})	Flexural strength (MPa)	Young Modulus (GPa)	Vickers Hardness (GPa)	Fracture Toughness (MPa $\sqrt{m}$)	Thermal conductivity (W/m K)	Thermal Shock Resistance ΔT (°C)	Coefficient of Thermal Expansion (10^{-6}/°C)
99	550–700	400	20.7	7–9	35	1000	6.8

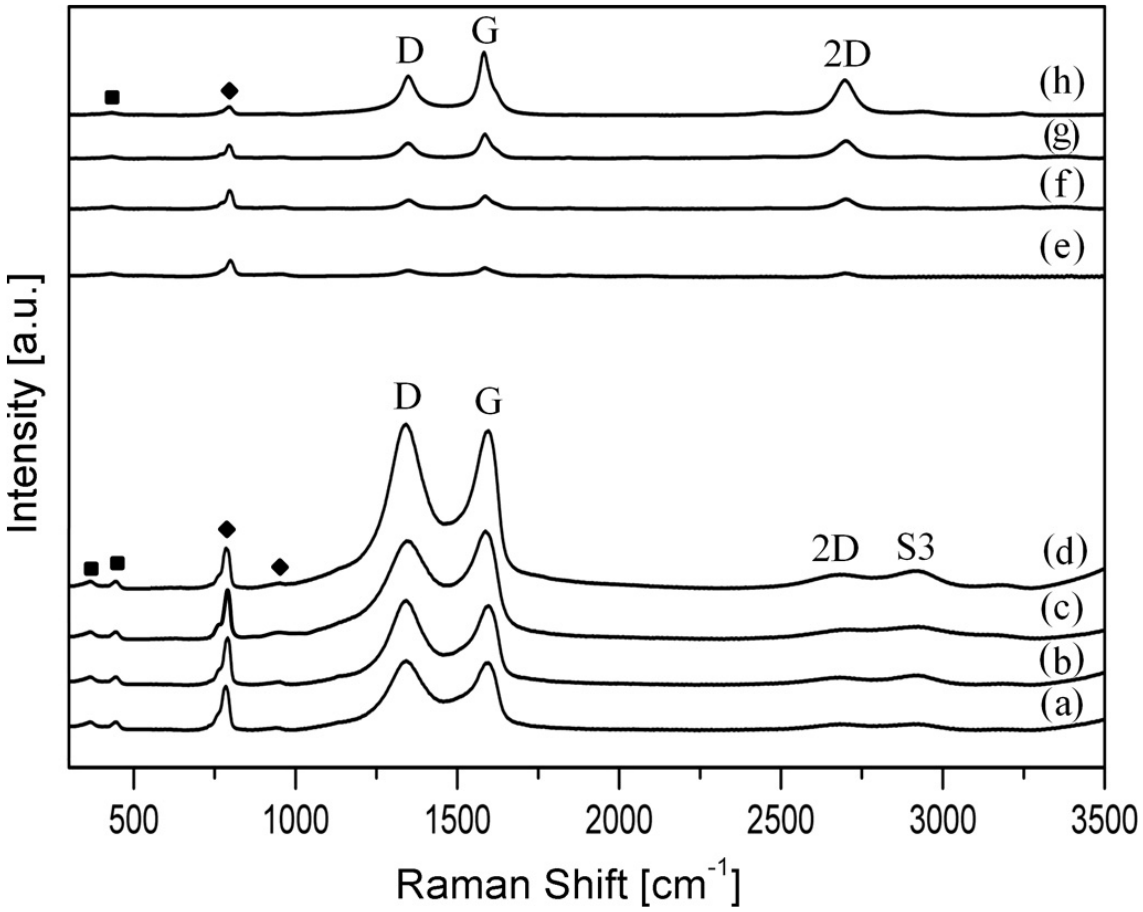

Fig. 1. Raman spectra of as-prepared Al2O3-SiCw-GO and sintered Al2O3-SiCw-Graphene composites containing 0.2 vol.% (a and e), 0.5 vol.% (b and f), 1 vol.% (c and g), and 5 vol.% (d and h) GO, respectively. "■" and "♦" labels denote alumina and silicon carbide peaks, respectively. "D", "G", "2D" and "S3" mark GO peaks before(a–d) and graphene peaks after (e–h) sintering, respectively.

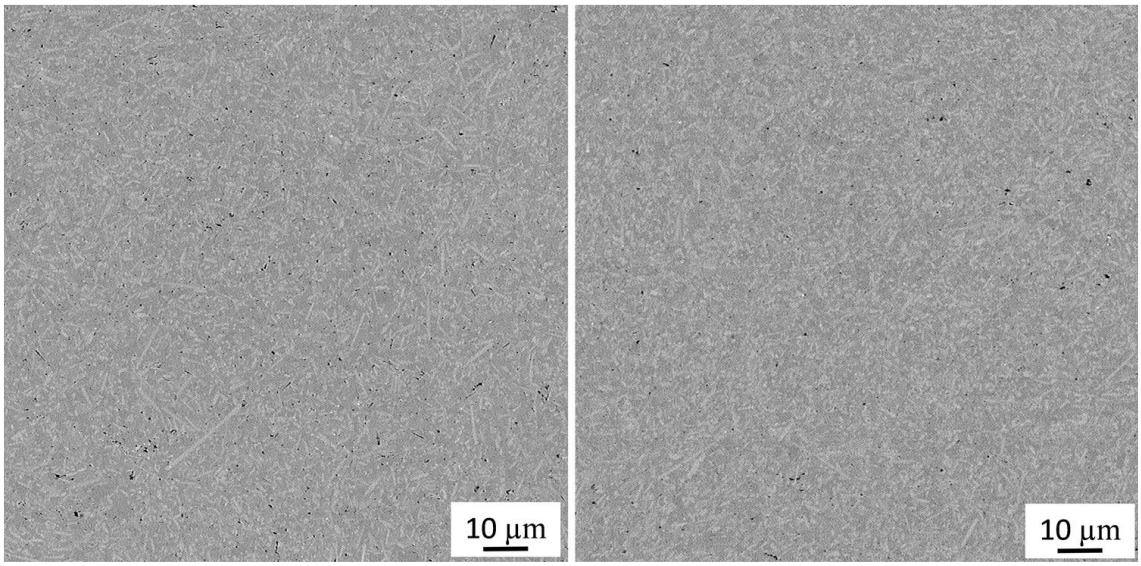

Fig. 2. SEM images of Al2O3–SiCw (left) and Al2O3–SiCw–0.5-G (right) polished composite surfaces

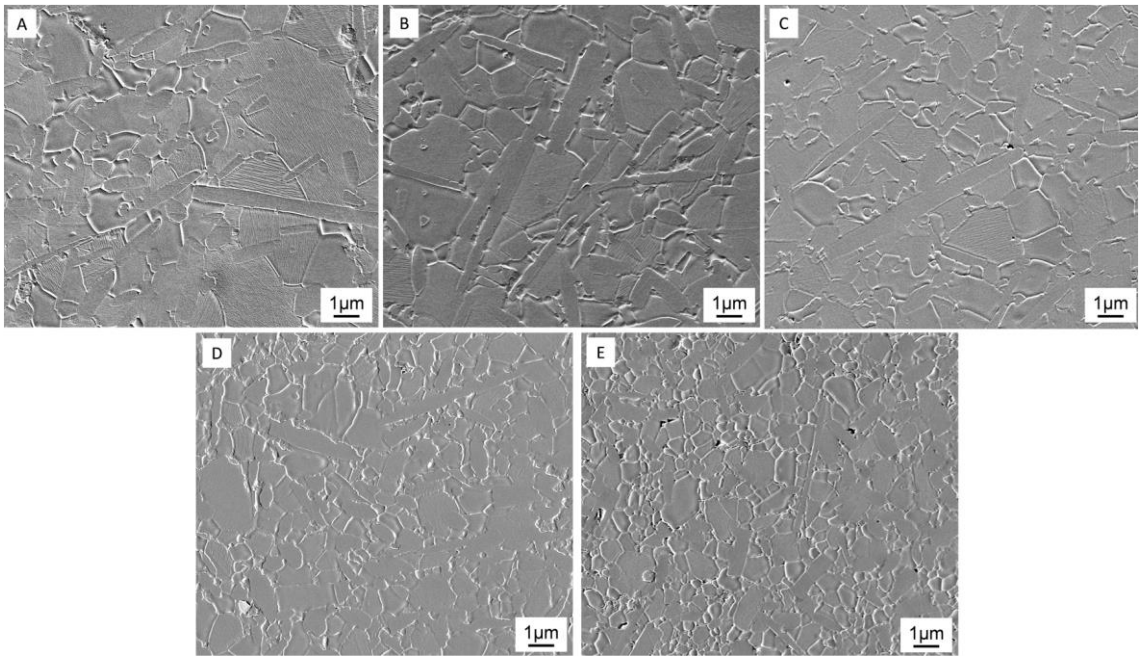

Fig. 3. SEM images of polished and thermally etched sections for 0-G (A), 0.2-G (B), 0.5-G (C), 1-G (D) and 5-G (E) sintered composites

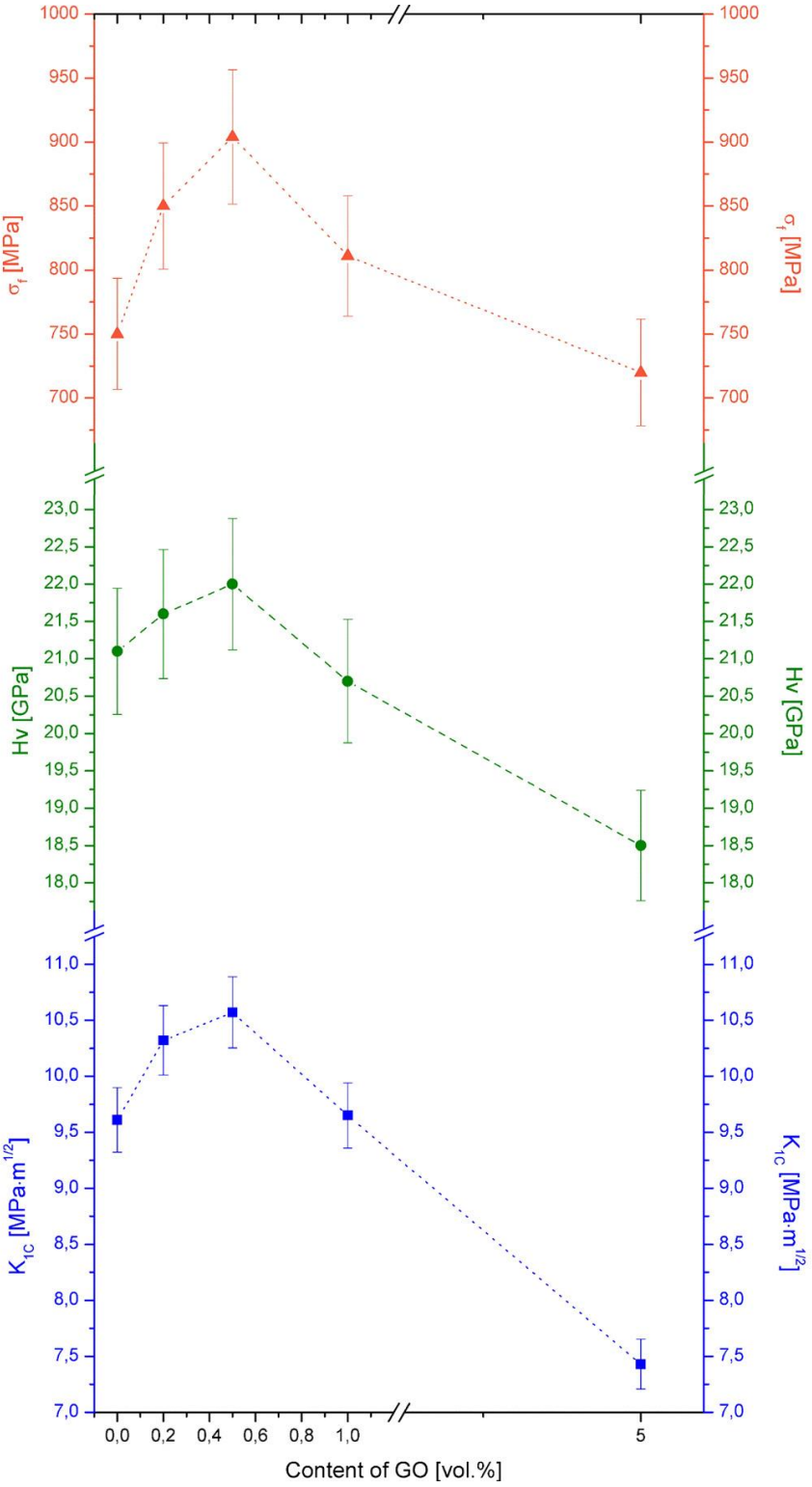

Fig. 4. Evolution of hardness, strength and fracture toughness of alumina-SiCw composites with different graphene oxide contents

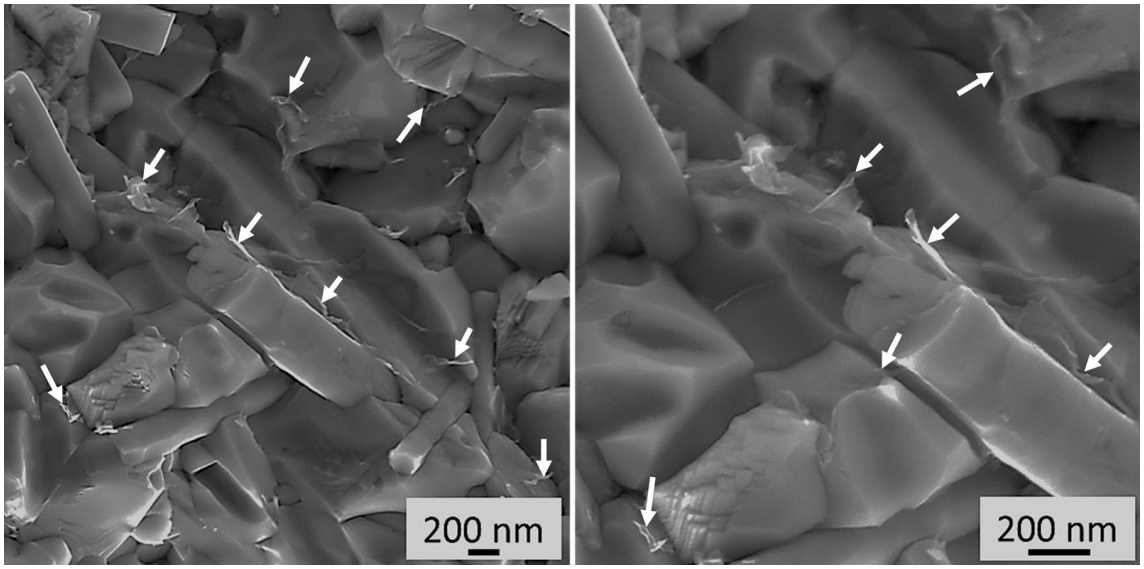

Fig. 5. SEM images showing the representative morphology of a 0.5-G ceramic composite fracture surface at low (left) and high (right) magnification. The white arrows illustrate the location of Graphene

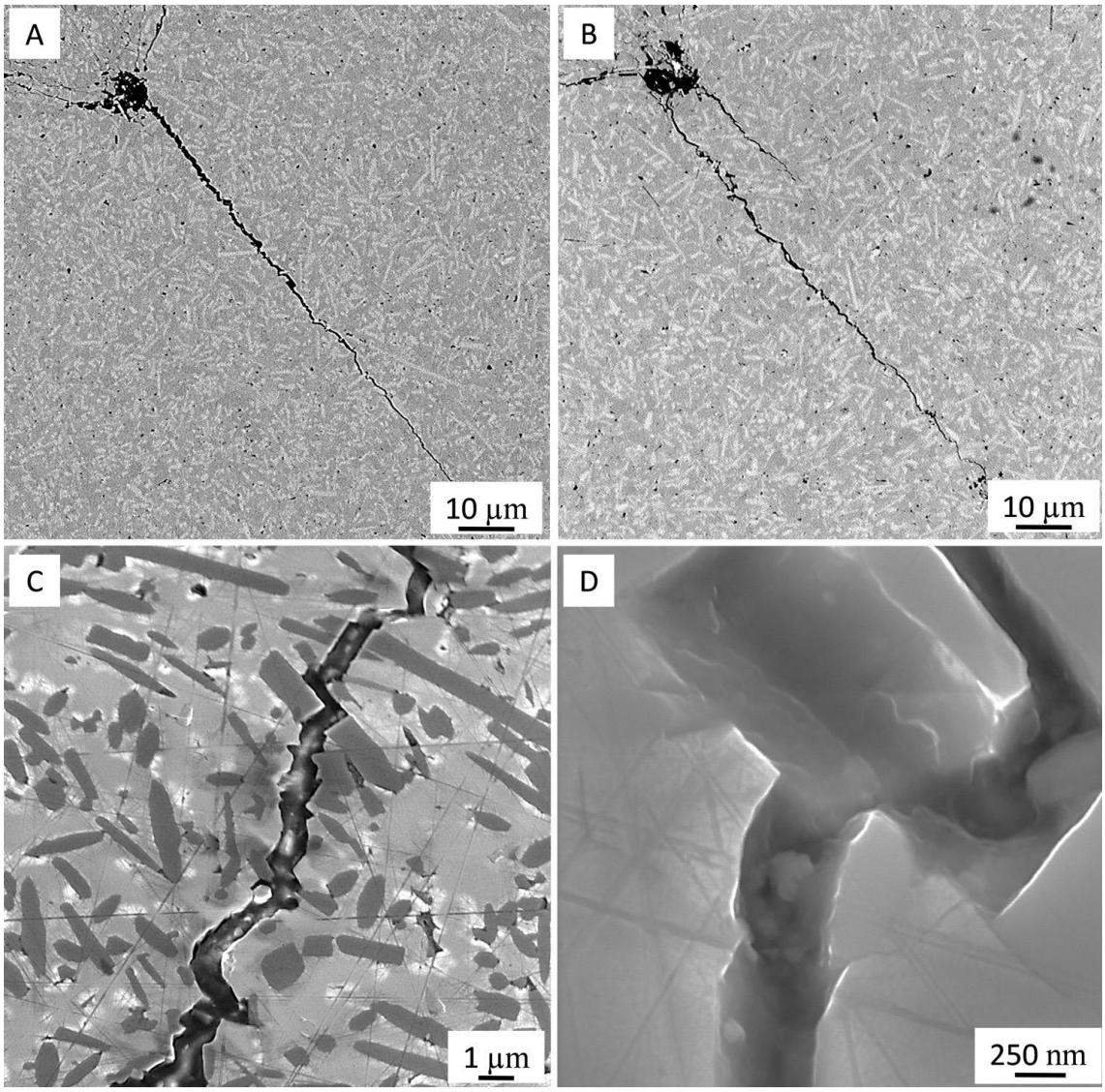

Fig. 6. Vickers indentation cracks induced on the surfaces of Ceramtuff (a) and 0.5-G (c, b, d) composites

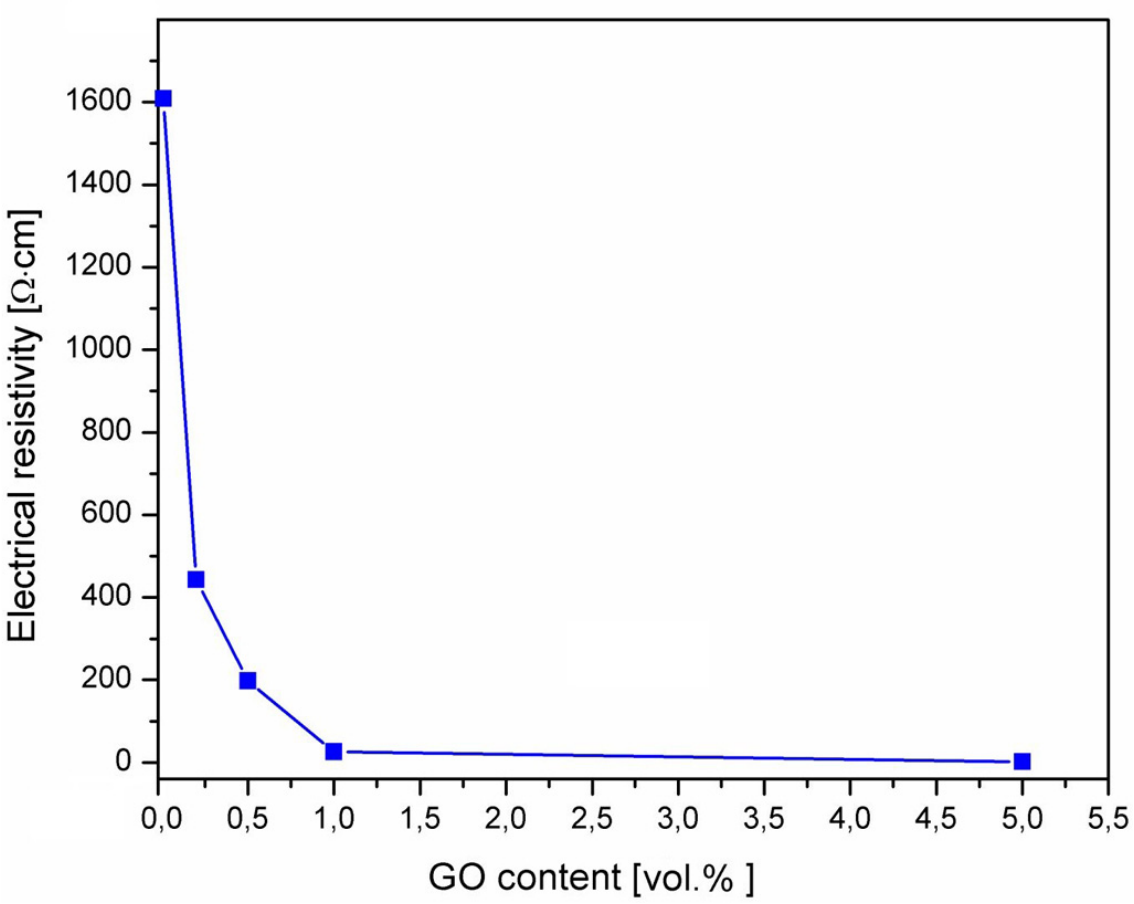

Fig. 7. The change in electrical resistivity of the sintered composites depends on the graphene content